

Phase Field Simulations of Autocatalytic Formation of Alpha Lamellar Colonies in Ti-6Al-4V



BALA RADHAKRISHNAN, SARMA GORTI, and SURESH SUDHARSANAM BABU

We present phase field simulations incorporating contributions due to chemical free energy, anisotropic interfacial energy, and elastic energy due to transformation strain, to demonstrate the nucleation and growth of multiple variants of alpha from undercooled beta in Ti-6Al-4V under isothermal conditions. A new composite nucleation seeding approach is used within the phase field simulations to demonstrate that the presence of a pre-existing strain field can cause the nucleation of specific crystallographic variants of alpha based on minimization of local elastic strain energy. Under conditions where specific combinations of elastic strains exist, for example in the vicinity of one or more pre-existing alpha variants, the nucleation of a new alpha variant is followed by the successive nucleation of the same variant in the form of a lamellar colony by an autocatalytic mechanism. At a given thermodynamic undercooling, the colony structure was favored at a nucleation rate that was low enough to allow sufficient growth of previously nucleated variants before another nucleus formed in their vicinity. Basket weave morphology was formed at higher nucleation rates where multiple nuclei variants grew almost simultaneously under evolving strain fields of several adjacent nuclei.

DOI: 10.1007/s11661-016-3746-6

© The Minerals, Metals & Materials Society and ASM International 2016

I. INTRODUCTION

THE microstructures of two-phase Ti alloys are composed of the β phase that has a body-centered cubic structure and the α phase that has a hexagonal close-packed structure. β is stable at high temperature and α precipitates in the form of plates from β on cooling. The existence of a Burgers orientation (BO) relationship between β and α given by

$$(101)_{\beta} \parallel (0001)_{\alpha}, [11\bar{1}]_{\beta} \parallel [11\bar{2}0]_{\alpha} \quad [1]$$

results in 12 possible variants of α based on the crystal symmetries of β and α .^[1] Two distinctly different microstructures are produced depending upon the undercooling of the β phase field. Typically, a basket weave structure is produced at a large undercooling where a high thermodynamic driving force favors the

intragranular nucleation and growth of multiple variants of α . When the undercooling is lower, a lamellar α in the form of colony morphology is obtained. Formation of the colony structure under these conditions has been mainly attributed to the formation of Widmanstätten side-plates (WS) of the same variant originating from a grain boundary allotriomorph (GBA) of α .^[2] The nucleation of WS occurs in general by one of the following mechanisms: (1) the instability of the GBA- β interface that grows with the same variant into a β grain that has BO relationship with GBA^[3] or (2) sympathetic nucleation^[4] of WS ahead of the GBA- β interface with a misorientation to account for the deviation of the β grain orientation from BO with respect to GBA. Recent phase field calculations^[5] have shown that the variant selection in the latter mechanism may be driven by the minimization of the elastic strain energy due to transformation strains and may be more appropriately considered as autocatalytic nucleation.

However, the mechanisms of WS based entirely on grain boundary nucleation may not be adequate to explain the formation of intragranular colony structure in coarse-grained materials. An interesting example is the formation of α colonies during laser additive manufacturing (LAM) of Ti-6Al-4V.^[6,7] Prior beta grains in this case are of the order of several millimeters, while the packet length of the α colonies is only of the order of 10 seconds of micrometers. Therefore, it is necessary to explore mechanisms by which α lamellae can be nucleated inside the β grains. In Ti-6Al-4V, nuclei of α that form inside the grains are known to be coherent with the β matrix and are known to nucleate heterogeneously in the strain fields of pre-existing

BALA RADHAKRISHNAN and SARMA GORTI, Senior Research Staff, are with the Oak Ridge National Laboratory, 1 Bethel Valley Rd, Oak Ridge, TN 37831. Contact email: radhakrishnb@ornl.gov SURESH SUDHARSANAM BABU, Professor, is with the Department of Mechanical, Aerospace and Biomedical Engineering, University of Tennessee, Knoxville, TN, 37996

This manuscript has been authored by UT-Battelle, LLC under Contract No. DE-AC05-00OR22725 with the U.S. Department of Energy. The United States Government retains and the publisher, by accepting the article for publication, acknowledges that the United States Government retains a non-exclusive, paid-up, irrevocable, world-wide license to publish or reproduce the published form of this manuscript, or allow others to do so, for United States Government purposes. The Department of Energy will provide public access to these results of federally sponsored research in accordance with the DOE Public Access Plan (<http://energy.gov/downloads/doe-public-access-plan>).

Manuscript submitted September 11, 2015.

Article published online September 13, 2016

dislocations.^[8] Therefore, it is possible to have variations in the nucleation rate of intragranular α due to variations in the prior dislocation density. Since the strain field of dislocations couple with the transformation strain field of the α variants, dislocations are able to selectively nucleate up to 5 variants at low levels of thermodynamic undercooling [1120 K (847 °C)], while at higher undercooling where the thermodynamic driving forces are higher [1020 K (747 °C)], it has roughly equal propensity to nucleate all 12 variants.^[8] Variation in nucleation rate due to dislocation density has been demonstrated during warm laser shock peening of aluminum alloy AA6061.^[9] In the current simulations, we assume that multiple variants are nucleating at dislocations at a rate proportional to the total dislocation density.^[10] At a given undercooling, it is possible to envision based on the pre-existing dislocation density: (1) a high nucleation rate where there is insufficient time for the growth of any one variant to offer a significant, unique strain field to induce a variant selection in another nucleus forming in its vicinity based on strain energy minimization, and (2) a lower nucleation rate where the first-to-form variants can grow to a large size before additional nucleation can occur in their vicinity such that the strain field of the pre-existing variant can significantly influence the subsequent variant selection when nucleation occurs in its vicinity. At the higher nucleation rate, the growth of multiple variants would occur in the presence of an evolving, long-range, complex strain field that stabilizes several variants through a strain accommodation mechanism, leading to the basket weave structure.^[11] However, when the nucleation rate is lower, the variant selection would become sensitive to the elastic strain energy associated with the growth of specific variants. In this case, the strain field due to the pre-existing variant could overcome the strain field of a single dislocation that was responsible for the formation of a nucleus. The presence of the strain field adjacent to the large, pre-existing variants could promote the autocatalytic nucleation of specific variants, very similar to the mechanism observed for the autocatalytic nucleation of an α colony from a pre-existing GBA.^[4] Although recent phase field simulations in Ti-6Al-4V have demonstrated the preferential formation of selective variants due to the strain field of a large, pre-existing α ,^[5] the simulations have not demonstrated the formation of a colony microstructure. Intragranular nucleation of α lamellae from pre-existing stacking faults has been demonstrated in gamma titanium aluminide.^[12]

The objective of this study is to simulate the $\beta \rightarrow \alpha$ diffusional transformation in Ti-6Al-4V using a phase field method. Initially, the growth of isolated, individual α variants in a β grain is simulated and the variant morphology and crystallographic orientation are compared with existing results^[5] to validate the method. Subsequently, the phase field approach is coupled with a unique composite nucleation model that is capable of capturing the effect of pre-existing strain field in β on the variant selection during nucleation of α . Finally, the nucleation and growth of multiple α variants in a large single crystal β are simulated at levels of thermodynamic

undercooling where dislocation-mediated nucleation is known to promote the formation of multiple variants of α .^[8] The nucleation rate at each undercooling was varied based on the assumption of different levels of prior dislocation density in β . The simulation results are analyzed in the context of a morphological change from a basket weave to a colony structure in Ti-6Al-4V during LAM.^[6,7]

II. SIMULATION APPROACH

In the phase field method, the individual phases and their crystallographic variants are described by a set of non-conserved order parameters. The interface between two phases or variants of a phase has a gradient in one of the order parameters that smoothly varies from 0 to 1 at the corresponding interface. Therefore, the technique is called a “diffuse interface” model. The method allows for capturing complex interface morphologies resulting from phase transformations without the need for tracking the interfaces explicitly, as in alternative techniques such as sharp-interface, front-tracking models. In addition to the order parameter gradient, there are also gradients in the local concentrations of solutes at the diffuse interface. The order parameters and the solute concentrations are coupled at the interface through thermodynamic and kinetic constraints. In the approach by Kim *et al.*,^[13] a parallel tangent approach was used to identify phase concentrations at the same chemical potential and the interface was assumed to consist of mixtures of the two phases. While the Kim *et al.*^[13] approach was developed for binary alloys, it was generalized to multi-component systems by Steinbach and Apel.^[14] Kobayashi *et al.*^[15] developed an approach where the interface region was assumed to consist of a mixture of two phases whose concentrations were determined by local thermodynamic equilibrium and therefore through a common tangent approach. Simulation of ternary alloys was carried out using this approach and linking the phase field simulations to a thermodynamic database. The approach used in the current simulations is the one by Kim *et al.*^[13] Comprehensive reviews of the phase field method and their applications in materials science can be found elsewhere.^[16,17]

In the current phase field model, the total free energy of the system per unit volume, F , is defined as

$$F = \int (F_{\text{ch}} + F_{\text{b}} + F_{\text{el}}) dV, \quad [2]$$

where F_{ch} is the chemical free energy per unit volume, F_{b} is the interfacial energy per unit volume due to grain and interphase boundaries, and F_{el} is the elastic energy per unit volume arising from transformation strains due to solid-state phase transformations. F_{ch} includes the contribution from the parent and the product phases in the microstructure. In the case of Ti-6Al-4V, there are 12 different variants of the product α phase along with the β matrix phase. Therefore, F_{ch} is given by

$$F_{\text{ch}}(T, X_k, \phi_p) = \sum_{p=1}^{12} h(\phi_p) F_v^\alpha(T, X_{\text{Al,V}}^\alpha) + \left(1 - \sum_{p=1}^{12} h(\phi_p)\right) F_v^\beta(T, X_{\text{Al,V}}^\beta), \quad [3]$$

where F_v^α and F_v^β are the free energy per unit volume of the α and β phases, respectively, and $h(\phi)$ is an interpolation function of the order parameter given by

$$h(\phi) = \phi^3(6\phi^2 - 15\phi + 10). \quad [4]$$

$h(\phi)$ has the property that it is equal to 1 when $\phi = 1$ and 0 when $\phi = 0$. The boundary energy, F_b , is given by the sum of the energy of the diffuse interface and an additional penalty due to the presence of a gradient at the diffuse interface as shown below:

$$F_b = \frac{1}{2} \sum_{p=1}^{12} [\nabla\phi_p]^T \kappa_p [\nabla\phi_p] + \sum_{p=1}^{12} \sum_{q>p} \omega_{pq} |\phi_p \phi_q| + \bar{\omega} \sum_{q=1}^{12} \phi_q \left(1 - \sum_{p=1}^{12} \phi_p\right). \quad [5]$$

In Eq. [5], the first term is the gradient energy with anisotropic gradient coefficient, κ , and the 2nd and 3rd terms together describe the energy of the α - α and α - β boundaries in the system, where ω is an energy-well calculated using the boundary width and the average gradient coefficient. The free energies of α and β phases as a function of Al and V concentrations (X_{Al} and X_{V} , respectively) at different temperatures were obtained from Thermo-CalcTM using the TTTI3 database (Ti Alloys Database V3) with Al concentration ranging from 0.0 to 0.20 wt pct, and V concentration ranging from 0.0 to 0.40 wt pct. The free energy values were fitted to a second-degree polynomial in X_{Al} and X_{V} for different temperatures. The error between the Thermo-CalcTM data and the fit was between 0.1 and 1 pct over the range of the Al and V concentrations.

In phase field simulations of solid-state phase transformations, the elastic energy, F_{el} , can be computed using several approaches. An approach that is commonly used is to utilize a closed-form solution to the coherent elastic energy based on the homogeneous elasticity theory of Khachaturyan.^[18] In addition, there are three main approaches that explicitly consider the elastic inhomogeneity between the matrix and the precipitate. The three approaches differ in the way in which the elastic strains and stresses are described in the diffuse interface between the matrix and the precipitate. In all three models, the elastic strain $\varepsilon_{kl}^{\text{el}}$ is defined as $\varepsilon_{kl}^{\text{tot}} - \varepsilon_{kl}^*$, where ε_{kl}^* is the strain that arises due to phase transformation and $\varepsilon_{kl}^{\text{tot}}$ is the total strain given by $\bar{\varepsilon}_{kl} + \delta\varepsilon_{kl}$, where $\delta\varepsilon_{kl}$ is the lattice inhomogeneous strain due to displacements. In the Khachaturyan inhomogeneous elasticity model,^[18] the strain energy is described as $F^{\text{el}} = \frac{1}{2} \varepsilon_{ij}^{\text{el}} : C_{ijkl} : \varepsilon_{ij}^{\text{el}}$, where the stiffness matrix, C_{ijkl} is defined as $h(\phi)C_{ijkl}^\alpha + [1 - h(\phi)]C_{ijkl}^\beta$, and the transformation strain ε_{kl}^* is

defined as $h(\phi)\varepsilon_{kl}^{*,\alpha} + [1 - h(\phi)]\varepsilon_{kl}^{*,\beta}$. In other words, stiffness matrix and the strains are interpolated across the diffuse interface. In another scheme by Steinbach and Apel,^[14] the strain energy is interpolated over α and β phases as $F_{\text{el}} = h(\phi)F_{\text{el}}^\alpha + [1 - h(\phi)]F_{\text{el}}^\beta$, where the strain energy in the individual phases is calculated separately using their respective elastic constants according to $F_{\text{el}}^\alpha = \frac{1}{2} \varepsilon_{ij}^{\text{el},\alpha} : C_{ijkl}^\alpha : \varepsilon_{ij}^{\text{el},\alpha}$ and $F_{\text{el}}^\beta = \frac{1}{2} \varepsilon_{ij}^{\text{el},\beta} : C_{ijkl}^\beta : \varepsilon_{ij}^{\text{el},\beta}$. The overall elastic strain $\varepsilon_{kl}^{\text{el}}$ (defined as $\varepsilon_{kl}^{\text{tot}} - \varepsilon_{kl}^*$ where $\varepsilon_{kl}^{\text{tot}}$ is the total strain and ε_{kl}^* is the transformation strain) is interpolated between α and β as $\varepsilon_{kl}^{\text{el}} = h(\phi)\varepsilon_{kl}^{\text{el},\alpha} + [1 - h(\phi)]\varepsilon_{kl}^{\text{el},\beta}$. In a third approach by Voigt and Taylor,^[19] the total strain is assumed to be the same in all phases at the interphase, and the elastic stress is interpolated between α and β . In the current simulations, the Steinbach–Apel approach was used for calculating the elastic energy due to transformation strain. Assuming mechanical equilibrium, the displacements in α and β phases were calculated using an iterative technique proposed by Hu and Chen.^[20] The elastic constants for α and β were obtained from.^[21]

The evolution of the system is due to a reduction in the total free energy, F , and is obtained by solving the Ginzburg-Landau and Cahn-Hilliard equations for the non-conserved order parameters for the 12 α variants, ϕ_p , and the conserved species concentrations, X_{Al} and X_{V} , respectively. Detailed description of the phase field technique for solid-state transformations is well documented in the literature and we describe only some of the specific features of our approach. The form of the Ginzburg-Landau equation that relates the partial derivative of the order parameter with respect to time to the functional derivative of the system energy with respect to the order parameter used in the current simulations is given by^[5]

$$\frac{\partial\phi_p(r, t)}{\partial t} = -L \left\{ \frac{1}{\bar{N}} \sum_{p \neq q} \left(\frac{\delta F}{\delta\phi_p(r, t)} - \frac{\delta F}{\delta\phi_q(r, t)} \right) \right\}. \quad [6]$$

In Eq. [6], the quantity L is the mobility of the diffuse interface. In the current simulations, it was calculated at a given temperature using an approach developed by Kobayashi *et al.*^[15] for the solidification of a ternary alloy. The quantity \bar{N} is the number of phases that coexist at any point, which in our simulations was determined using a cut-off value for the order parameters of 0.05. Eq. [6] is solved for each α variant with order parameter ϕ_p , with the constraint that $\sum_{p=1}^{12} \phi_p + \phi_m = 1.0$ at any point, where ϕ_m is the order parameter for the matrix. The 12 variants of α bear a BO relationship with β , and their orientations were obtained using the procedure outlined in Reference 5. The numbering scheme used for the variants in the current simulations is identical to the one used in Reference 5. The interfacial anisotropy and the transformation strains for the variants were also obtained from Reference 5. The Cahn-Hilliard equation used in the simulations was based on an extension of the form used by

Kim *et al.*^[13] for binary alloys to the ternary Ti-6Al-4V alloy. The final form of the Cahn-Hilliard equation used in the present simulations is as given below for Al concentration, and a similar expression can be written for V concentration.

$$\begin{aligned} \frac{\partial X_{Al}}{\partial t} = & \nabla \cdot [D_{Al} \nabla X_{Al} + D_{Al} \lambda \nabla X_V \\ & + D_{Al} \sum_{p=1}^{12} \{h'(\phi_p) (X_{Al}^\beta - X_{Al}^\alpha) \\ & + h'(\phi_p) (X_V^\beta - X_V^\alpha) \lambda\} \nabla \phi_p]. \end{aligned} \quad [7]$$

In Eq. [7], the quantity λ is given by

$$\lambda = \frac{\partial^2 F_v^\alpha / \partial X_{Al}^\alpha \partial X_V^\alpha}{\partial^2 F_v^\alpha / \partial (X_{Al}^\alpha)^2} \quad [8]$$

A. Assumptions

Under low thermodynamic undercooling, the rate-limiting step for the $\beta \rightarrow \alpha$ transformation is the diffusion of V in the β phase, since V is the slow diffuser.^[22] As the undercooling increases, the sharp concentration peak that builds up in the β phase on cooling to the undercooling temperature is known to result in the formation of a face-centered cubic, interface phase.^[23] This leads to a reduction in the V concentration on the β side and enrichment on the α side of the interface that effectively reduces the partitioning of V between β and α . However, the extent of undercooling and the actual interface V concentrations are not known. Moreover, phase field simulations that include the interface phase and its evolution during growth are too complicated, and not the main focus of this study. Therefore, the diffusion of V is not considered and we assume that the $\beta \rightarrow \alpha$ transformation is controlled by Al diffusion with no partitioning of V. In addition, there is further supporting evidence that V diffusion may not play a significant role during short isothermal holds of a few seconds that are the subject of this present investigation. Ohmori *et al.*^[24] performed isothermal studies at different levels of undercooling and performed compositional analysis of β and α phases using wavelength dispersion spectroscopy. They concluded that for short isothermal holds of 20 seconds at 1173 K (900 °C), the partitioning of V was quite insignificant, and that significant partitioning occurred only at isothermal hold times of the order of several minutes. Ahmed and Rack^[25] used an

instrumented Jominy test to investigate $\beta \rightarrow \alpha$ transformation in Ti-6Al-4V under cooling rates ranging from 410 to 1.5 K/s. Through careful morphological and analytical electron microscopy characterizations, they concluded that a diffusionless, massive transformation of $\beta \rightarrow \alpha$ occurred down to cooling rates of roughly 20 K/s. As the cooling rate was further reduced, the transformation seemed to occur by an interfacial diffusion mechanism and ledge-wise diffusional growth. More recently, Ji *et al.*^[26] performed a theoretical assessment of phase transformation kinetic pathways in Ti-6Al-4V using a graphical thermodynamic approach. The analysis showed that for isothermal transformation in the temperature range of 895 K to 1145 K (622 °C to 872 °C) $\beta \rightarrow \alpha$ initially occurred *via* diffusionless nucleation followed by a diffusional nucleation and growth of the $\alpha \rightarrow \alpha + \beta$ transformation. The phase field simulations in the present work have been carried out isothermally at 950 K or 1000 K (677 °C or 727 °C) that fall in the above temperature range. The diffusion coefficient for Al used in the simulations was taken from Semiatin *et al.*^[27] The impurity diffusion coefficient of Al in α and β have been published by Good.^[28] The diffusion coefficients are shown in Table I. It is clear that the relative diffusivity of Al in α and β is roughly the same. This allowed us to assume equal Al diffusivity in α and β that simplified the phase field solution to Eqs. [7] and [8].

B. Numerical Approach

Equations [6] and [7] were solved using a semi-implicit, Fourier spectral method proposed by Shen and Chen^[29] using periodic boundary conditions. A parallel three-dimensional fast Fourier transform library, P3DFFT, that allows domain decomposition to be carried out in two orthogonal directions,^[30] was used to implement the solution in a parallel computing environment so that large simulation volumes could be handled. Table II summarizes the parameters used in the phase field model.

C. Nucleation Model

One of the challenges in phase field simulations is to accurately incorporate the nucleation step. The nucleation step in phase field simulations is typically carried out using either a Langevin noise, which is introduced in the form of a stochastic perturbation term in the Ginzburg-Landau and the Cahn-Hilliard equations,^[5] or explicit Poisson seeding^[31] approach, where a critical, pre-determined fluctuation in the order parameter, composition, and shape with a diffuse interface is

Table I. Diffusion Coefficients of Al and V in Ti Solid Solution

Element	Phase	Diffusion Equation	Diffusivity $\times 10^{16}$ m ² /s	
			950 K (677 °C)	1000 K (727 °C)
Al	β	$D = 2.4 \times 10^5 \exp(-18040/T(K))$ [Ref. 27]	6.79	17.56
Al	α	$\ln(D) = -11.04 - 23700/RT(°C)$ [Ref. 28]	61.39	114.6
Al	β	$\ln(D) = -11.11 - 21900/RT(°C)$ [Ref. 28]	147.63	262.7

Table II. Parameters Used in the Phase Field Simulations of Ti-6Al-4V

Parameter	Values
Temperature	950 K (677 °C), 1000 K (727 °C)
Grid spacing	950 K (677 °C) – 1.7×10^{-8} m 1000 K (727 °C) – 1.9×10^{-8} m
Interface width	5 times grid spacing
Interfacial energy	0.4, 0.05, 0.1 J/m ² (anisotropic, in the local coordinate of the variant)
Interface mobility	obtained using Kobayashi <i>et al.</i> ^[15]
Transformation strains for 12 α variants	from Shi and Wang 2013 ^[5] (same numbering scheme used here for the variants)
Critical nucleus size (radius in lattice units)	950 K (677 °C) – 2.0 1000 K (727 °C) – 4.0
Elastic constants of α (GPa)	$C_{11} = 119.0, C_{12} = 64.0, C_{44} = 36.0, C_{33} = 134.0, C_{13} = 49.0$ ^[21]
Elastic constants of β (GPa)	$C_{11} = 97.7, C_{12} = 82.7, C_{44} = 37.5$ ^[21]
Diffusion coefficient of Al	$D = 24 \times 10^4 \exp(-18040/T) \mu\text{m}^2/\text{s}$ ^[27]

introduced based on the calculated nucleation rate. Even though Langevin noise approach works reasonably well at high undercooling where small fluctuations become critical, it is somewhat limited in physical insight. The explicit nucleation approach better captures the size and number density of the critical nuclei. However, it becomes very difficult to implement when there are additional complexities due to the presence of multiple crystallographic variants and variant selection based on dynamically varying strain fields. This is particularly relevant to Ti-6Al-4V where there are 12 crystallographic variants of α and the strain energy associated with nucleation of each variant could be different because of the presence of an evolving, long-range, strain field due to the presence of other pre-existing α variants.

In order to overcome the above complexities, a novel, composite nucleation approach was used in the current simulations. The composite nucleation model is roughly analogous to the multiple-variant nuclei forming at dislocations. It was shown in Reference 8 that the subsequent growth of such a complex of dislocation-nucleated variants will be influenced by strain fields arising from pre-existing variants. Instead of explicitly simulating the multiple-variant nuclei formation at dislocations, it was assumed that these composite nuclei would form at a frequency proportional to the dislocation density that exists in the material. In addition, the critical nucleus size for a composite was calculated in a strain-free β by simulating the evolution of an isolated spherical particle of α of a specific variant, and identifying the particle size that would transition from dissolution to growth mode for a given undercooling. It was assumed that the critical nucleus size of the composite nucleus was the same as that calculated using a single variant in a strain-free matrix. Therefore, the criterion used for placing the composite nuclei is quite approximate since it lacks the details of their evolution in the presence of the strain field of the dislocations. However, the dislocation nucleation simulations in Reference 8 could in future studies be coupled with the current simulations to get a more physical representation of the nucleation rate of the composite nuclei. Composite nuclei were introduced within the β phase

only if none of the order parameters belonging to the α variants at the location exceeded a low critical value. In the current simulations, the critical value used was 0.05, thus ensuring that the nuclei did not overlap with a pre-existing α . Such a procedure resulted in a decrease in the success rate of placing the composite nucleus because of the increasing transformed volume with simulation time. For each lattice site within the composite nucleus, the order parameter for each variant of α was assigned the value of 1/12, so that the sum of the order parameters for all variants at any site is equal to 1.0. Therefore, each sphere represented a composite nucleus that contained an equal fraction of each of the 12 variants, and its further evolution was determined by the growth of the variant(s) that minimized local energy while growing in the presence of strain fields of other variants causing subsequent variant selection.

The nucleation rate for heterogeneous nucleation of a coherent phase in the strain field of a dislocation is known to be proportional to the dislocation density.^[9,10] Accurate calculation of nucleation rate for a given thermodynamic undercooling is difficult because of the uncertainty in the pre-exponential terms.^[9,10] Therefore, we simply considered two arbitrary attempt frequencies, namely 0.4 and 5.0 s⁻¹ in the simulations. For example, for an attempt frequency of 0.4 s⁻¹, an attempt was made to place a composite nucleus into the simulation volume after every 2.5 seconds of simulation time. At transformation temperatures of 950 K and 1000 K (677 °C and 727 °C), these attempt frequencies resulted in almost complete transformation of β in about 45-50 seconds. Such transformation times are typical of Ti-6Al-4V where basket weave structure forms inside prior β grains.

III. SIMULATIONS

The following simulations were performed using the phase field approach described in the previous section:

- (1) Isothermal simulations at 950 K (677 °C) to capture the morphology, and spatial orientation of each of the 12 α variants in β matrix; these

simulations were carried out in a $128 \times 128 \times 128$ site simulation box with a critical spherical nucleus of radius 2 and a spatial resolution of 1.7×10^{-8} m.

- (2) Simulations of variant selection from a composite nucleus due to the presence of a pre-existing α variant; the α variant was introduced in the form of a vertical wall in the middle of the simulation box. Note that the orientation of the α wall is not the equilibrium orientation of the variant but it is parallel to the xz plane of the simulation coordinate system. The lateral stability of the wall during the simulations was artificially imposed by not allowing plane to evolve from the side faces. The objective of these simulations is merely to show that (a) the composite nucleation model is able to capture the effect of a pre-existing strain field on variant selection. These simulations were carried out isothermally at 1000 K (727 °C) in a $128 \times 128 \times 128$ site simulation domain.
- (3) Simulations of variant selection from a composite nucleus due to the presence of a pre-existing α variant; however unlike in Eq. [2] above, the variants are now present in their equilibrium orientations inside the β with no grain boundaries being present. The objective is to show that strain energy minimization at the potential nucleation site drives selection of a specific variant from the composite nucleus. These simulations were carried out in $64 \times 64 \times 64$ site domain with at 1000 K (727 °C).
- (4) Simulations of $\beta \rightarrow \alpha$ transformation at 950 K and 1000 K (677 °C and 727 °C) using composite nucleation model, assuming a nucleation attempt frequency of 0.4 or 5.0 s^{-1} at either temperature. These simulations were carried out in a simulation box of $256 \times 256 \times 256$ sites with a spatial resolution of 1.7×10^{-8} m [at 950 K (677 °C)] or 1.9×10^{-8} m (at 1000 K (727 °C)).

IV. RESULTS AND DISCUSSION

A. Growth of Isolated Precipitates

The crystallographic framework used to capture the BO relationship between the β matrix and the 12 variants of α is similar to the one developed by Shi *et al.*^[32] The three non-coplanar vectors that define the cubic coordinate system for the body-centered cubic β matrix are given by $x = [010]_{\beta}$; $y = [\bar{1}01]_{\beta}$; $z = [101]_{\beta}$ that also represents the crystallographic orientation of the computational frame. The transformation strain for each variant is calculated on the basis of the total lattice distortion due to a coherent transformation and the distortion due to the introduction of misfit dislocations and structural ledges on the precipitate-matrix interface. The misfit strains for different variants are obtained by rotation of the respective strain tensors to the computational frame.^[5,32] The interfacial energies for the side, edge, and broad faces of the precipitate are defined in

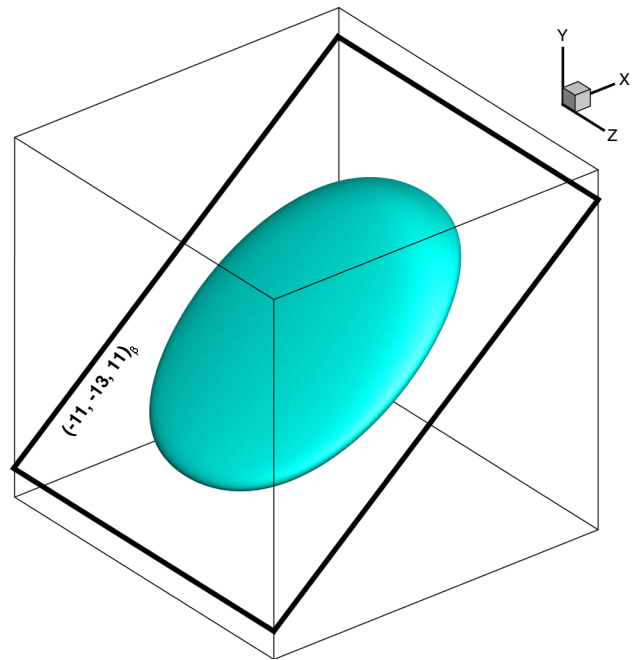


Fig. 1—Morphology of variant 1^[5] obtained using the simulations. The precipitate face is parallel to the habit plane in agreement with the simulations in Ref. [5].

the local coordinate system defined by the non-coplanar vectors $[x = [101]_{\beta}]$, $y = [\bar{3}, 5, 3]_{\beta}$ and $z = [\bar{1}\bar{1}, \bar{1}\bar{3}, 11]_{\beta}$. The anisotropic interfacial energies normal to these three interfaces (shown in Table II) are transformed to the computational domain. The variant morphology and the habit plane are shown in Figure 1 for one of the variants. The broad side of the precipitate is parallel to the habit plane, $[\bar{1}\bar{1}, \bar{1}\bar{3}, 11]_{\beta}$ in agreement with the results shown by Shi and Wang.^[5] The spatial orientations and morphology for all 12 variants are shown in Figure 2.

Figure 3 shows the temporal evolution of a single α variant (variant number 8) as a function of the simulation time at 950 K (677 °C). The simulation is started by placing a nucleus of radius 2.0 at the center of a $128 \times 128 \times 128$ computational domain with a grid spacing of 1.7×10^{-8} m. The order parameter corresponding variant 8 is set to 1.0, while all the other 11 order parameters are set to 0.0 within the spherical nucleus. The nucleus evolves by setting up a diffuse interface from the initial sharp interface that had a sharp discontinuity in the order parameter and by a change in shape from the initial sphere to the elongated morphology consistent with the equilibrium orientation of the variant and the interfacial energy. There is a simultaneous evolution of the order parameter and the concentration field within the matrix and the precipitate. The simulations are able to capture the Al depletion in the matrix side of the interface and the Al enrichment within the α variant. The depletion zone is confined to the broad face of the α , while it is absent along the sharp edges. This is presumably due to the higher interfacial

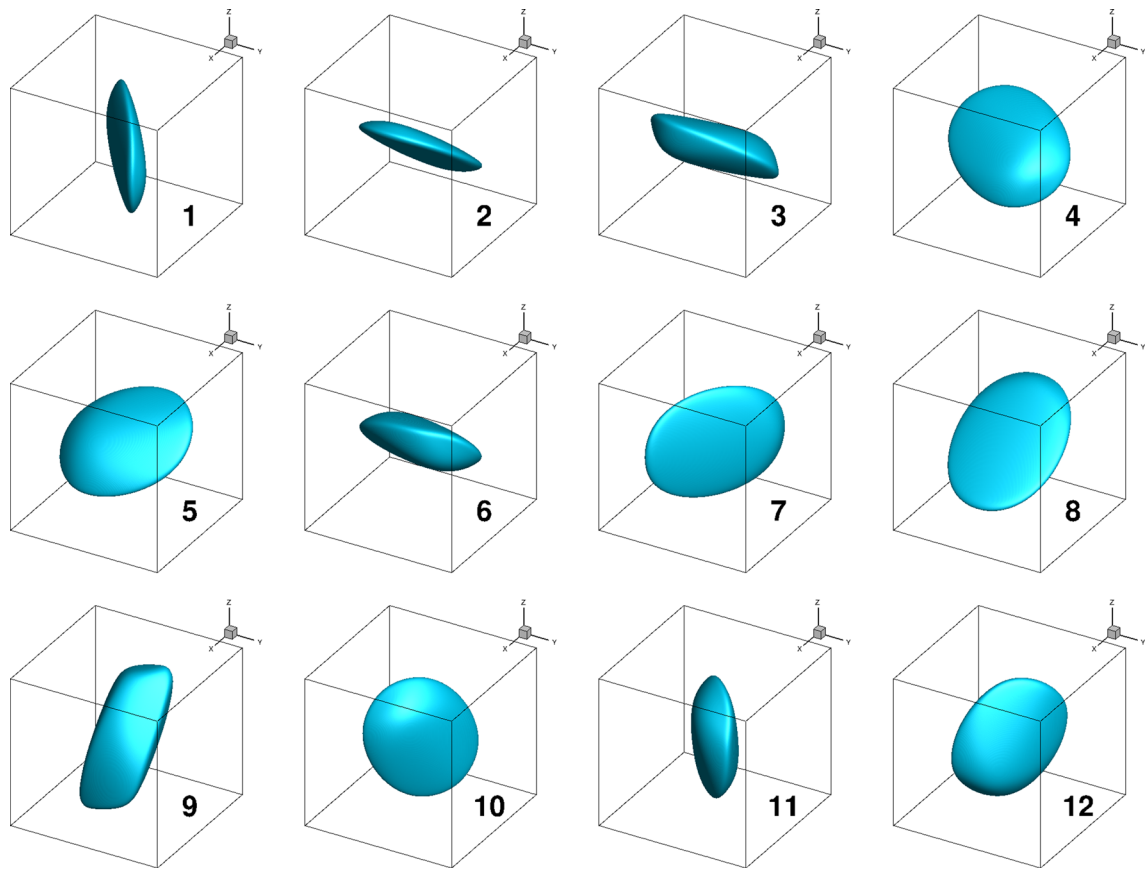


Fig. 2—Spatial orientation and morphology of α variants obtained from the phase field simulations. See Shi and Wang^[5] for an explanation of the variant numbers.

velocity at the edges than at the broad faces of the α precipitate.

B. Strain-Induced Variant Selection

Since the elastic energy generated by the growth of different crystallographic variants of α is the same when they are isolated, the selection of specific variants from a composite nucleus will occur only through the presence of a pre-existing strain field. The composite nucleus approach is quite efficient in capturing such an orientation selection as described below. In one set of simulations, the elastic strain field was introduced initially through a vertical wall of a single variant parallel to the yz plane of the simulation box positioned at the midsection along the x direction. Since the equilibrium orientation of the variant may not coincide with the wall direction, the wall is merely an artificial source for producing a strain field in the lattice. The vertical direction was chosen because continued growth of the wall variant by wrap around due to the periodic boundary conditions could be arrested. In addition, the lateral stability of the wall was ensured by artificially constraining the side surfaces of the wall. It is instructive to use this approach to illustrate the ability of the composite nucleus to evolve a selective orientation due to a pre-existing strain field. The composite nuclei are positioned

randomly along the y and z directions but restricted along the x direction to be very close to the interface between the variant wall and the matrix, so that each nucleus will fully experience the strain field due to the variant. Figures 4 and 5 show the results obtained for the presence of different variants in the wall. The simulations indicate that the presence of the strain field due to the wall preferentially nucleates specific variants from the composite nucleus.

Figure 4 shows two different kinds of selective nucleation from the composite nuclei due to the strain field of the wall. In one case, the variant in the wall selectively nucleates just one variant, while in the other case it nucleates two other variants out of the 12 possible variants. An example for the first case is shown in Figure 4(a) where variant 3 in the wall preferentially nucleates variant 4. Two examples are provided for the second case. When the variant in the wall is 4 (Figure 4(b)), it nucleates variants 3 and 5. Similarly, when the variant in the wall is 6, it nucleates variants 3 and 5 (Figure 4(c)). In Figure 4(a), while it appears that there are many precipitates of variant 4 that nucleated from the wall, in reality there are only two independently nucleated precipitates of variant 4 that wrapped around the faces of the simulation box due to the periodic boundary conditions used in the simulations.

Figure 5 shows an interesting case where the central wall with variant 5 first preferentially nucleates variants

2 and 6 from composite nuclei placed in the vicinity of the wall. However, unlike the cases shown in Figure 4, variant 10 nucleates at a later time from a composite nucleus placed in the vicinity of variants 2, 5, and 6, which then subsequently triggers the nucleation and growth of multiple parallel plates of variant 10 in the form of a colony due to the presence of the strain fields

from variants 2, 5, and 6. This is a clear example of colony formation by autocatalytic nucleation. Once the first plate of variant 10 formed, the additional plates in the colony formed quite frequently, with the result that the subsequent insertion of composite nuclei within the remaining space became an improbable event. While in this case, one of the variants (variant 5) was introduced

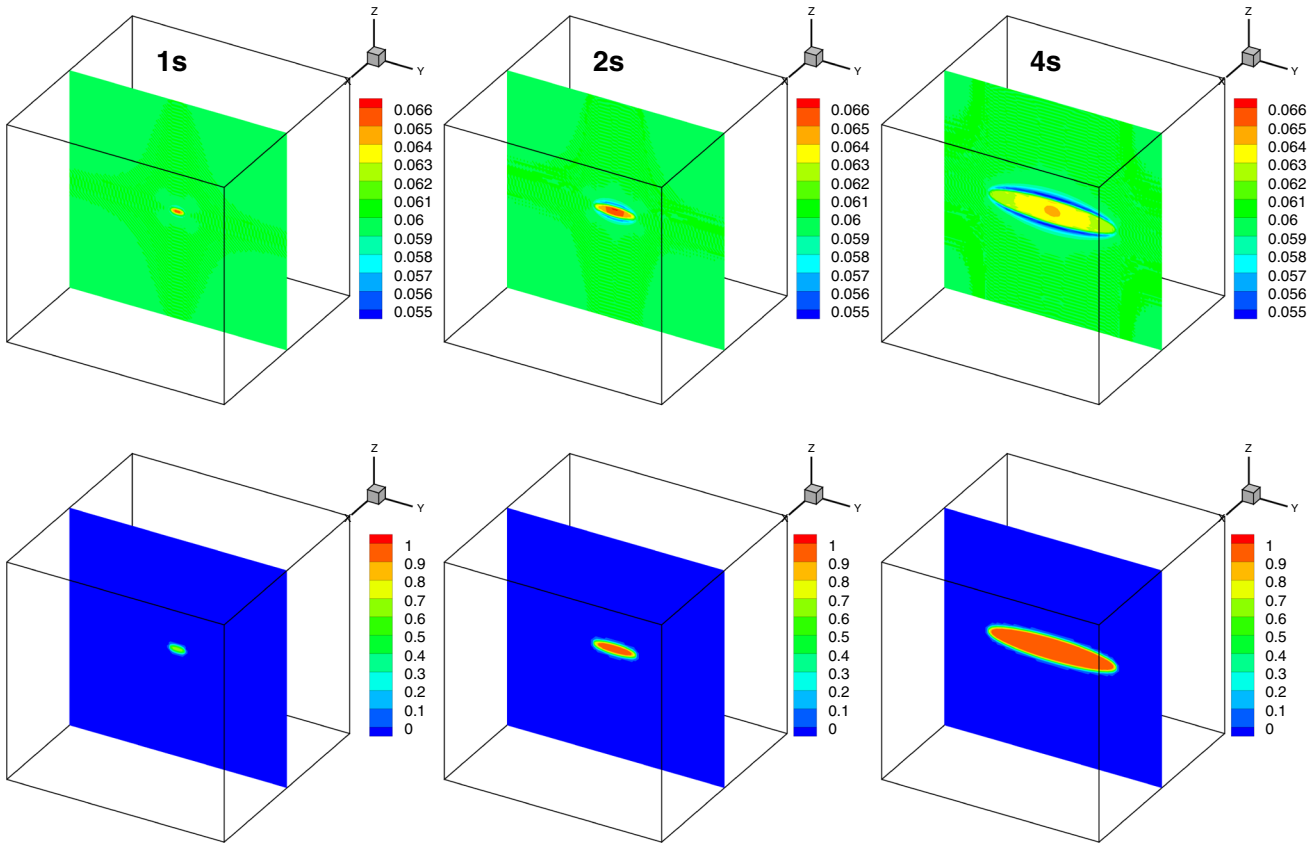


Fig. 3—Temporal evolution of variant 8 precipitating out of β showing evolution of Al concentration (top row) and order parameter (bottom row).

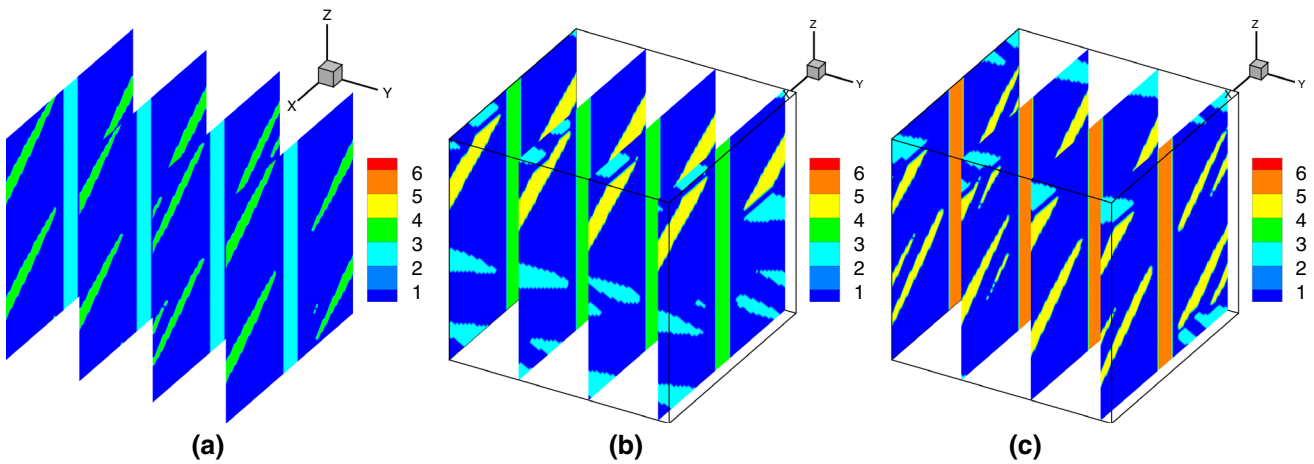


Fig. 4—Preferential nucleation from composite nuclei when they are placed in the vicinity of the strain field of a pre-existing variant in the form of a vertical wall parallel to the yz plane. (a) variant 3 in the wall nucleates variant 4, (b) variant 4 in the wall nucleates variants 3 and 5, and (c) variant 6 nucleates variants 3 and 5, from the composite nuclei. Colors are based on variant number.

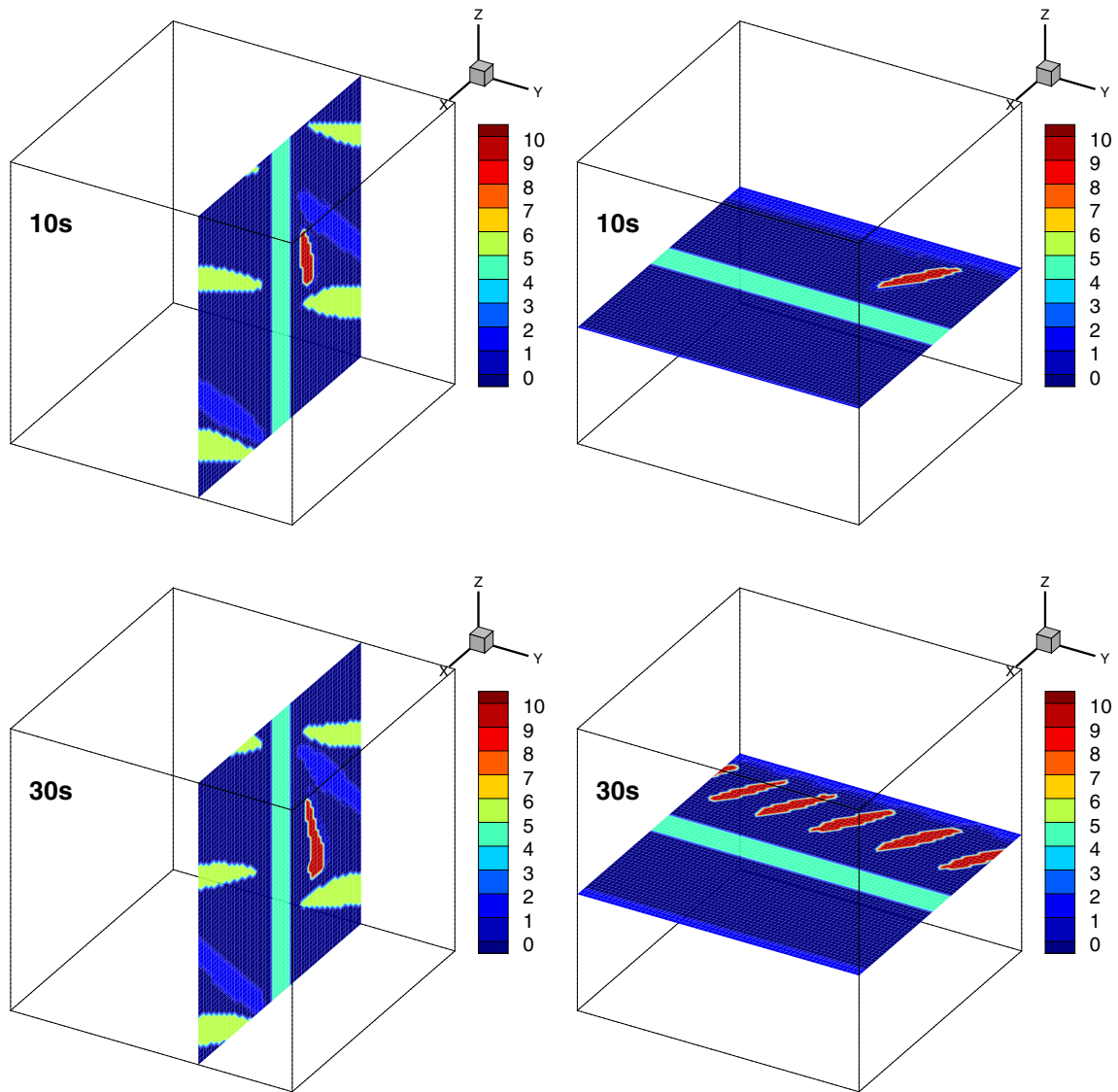


Fig. 5—Preferential nucleation of variant 10 from a composite nucleus in the presence of a wall with variants 6 and 2 nucleated earlier by the wall from composite nuclei (top row), and the subsequent autocatalytic nucleation and growth of variant 10 in the presence of the strain fields of variants 2, 5, and 6 (bottom row).

artificially in the form of a wall in a non-equilibrium position, the same mechanism operates when the three variants are present inside a grain in their equilibrium orientations satisfying the BO, as shown in the subsequent simulations.

In this simulation, variants 2, 5, and 6 were introduced initially through seeds of the respective variants. The 3 variants were then allowed to grow until subsequent growth was arrested by impingement. Composite nuclei were subsequently introduced in the strain field of variants 2, 5, and 6. The strain energy distribution due to the variants is shown in Figure 6(a) and the corresponding order parameter distribution is shown in Figure 6(b). Figure 6(d) shows the order parameter profile of a composite nucleus in the process of evolution. It is clear from Figure 6(c) that the evolution of the composite nucleus is accompanied by a reduction in the strain energy at that location.

Subsequent evolution of the strain energy and the order parameter profile are shown in Figures 6(e) and Figures 6(g) and Figures 6(f) and 6(h) respectively. It is clear that further evolution of the composite nucleus results in the formation of a single variant and in the process the strain energy in the corresponding volume decreases by the sweeping of the volume by a low-energy front. Figure 7 shows the morphology obtained at longer times after continued evolution of the newly formed variant. It is interesting to note that the variant that evolves in this case (variant 10) is the same as the one that nucleated in the previous example shown in Figure 5. Longer term evolution of this variant resulted in the formation of a lamellar structure by autocatalytic nucleation as before. As shown in Figures 6(g) and (h), the movement of the low-energy front causes the widening of the variant. As the strain energy increases due to widening, it is energetically favorable to nucleate

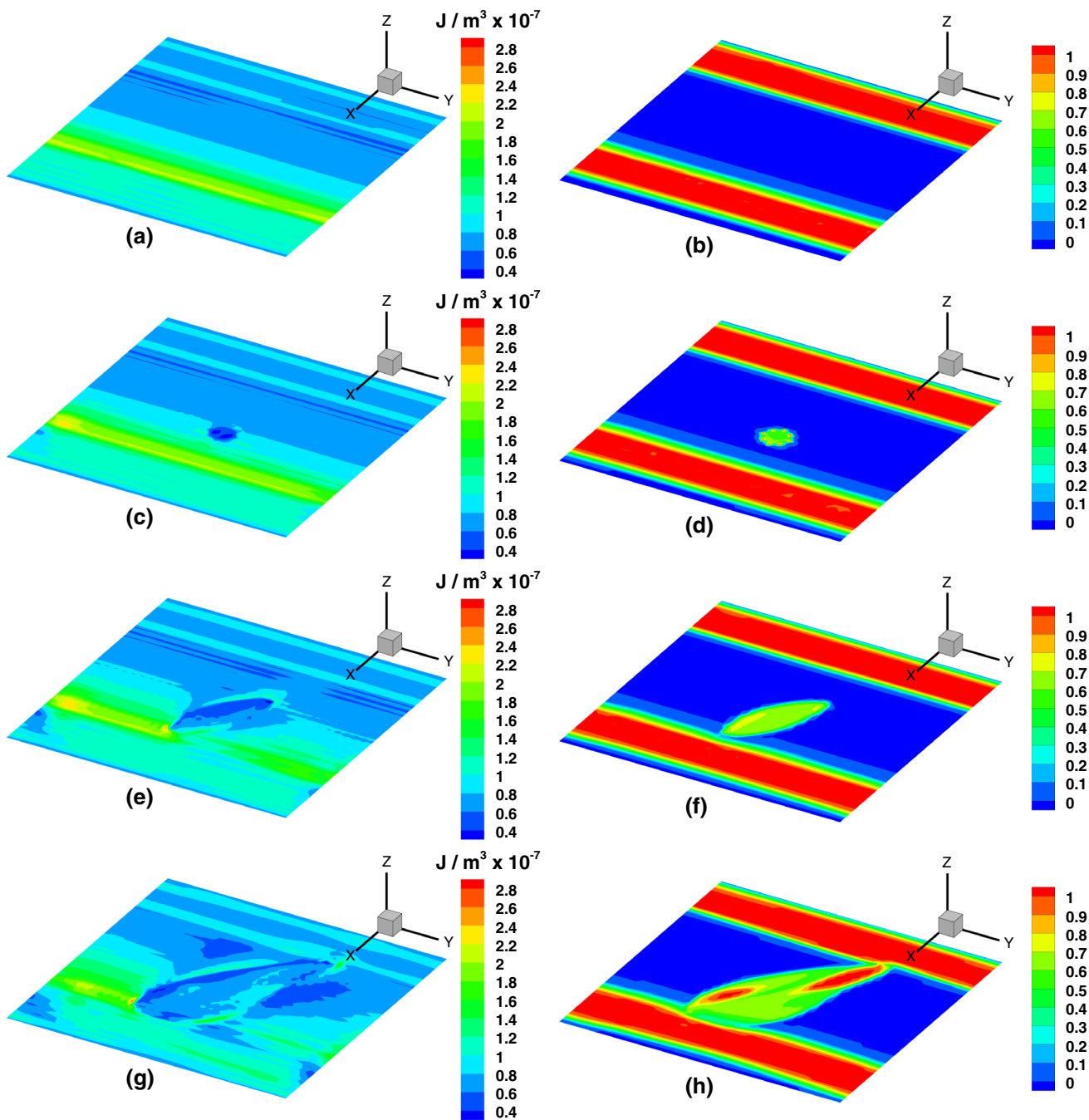


Fig. 6—Evolution of the elastic strain energy and order parameters during the evolution of a composite nucleus situated in the strain field of variants 2, 5, and 6. The strain energy locally decreases during the formation of a single variant from the composite nucleus as well as the subsequent autocatalytic nucleation of the variant by the sweeping of a low-energy front.

another variant, thus causing autocatalytic nucleation of the same variant in a columnar fashion.

C. Growth of Multiple α Variants

Isothermal simulations of α phase evolution in single crystal β through nucleation and growth were simulated at 950 K and 1000 K (677 °C and 727 °C) representing two levels of undercooling. A nucleation attempt frequency of 0.4 or 5 s⁻¹ was used as described previously

to account for materials with two different dislocation densities. Composite nuclei were introduced at random locations within the untransformed β matrix based on the overlap criterion described previously. If the random location fell in a region of overlap nucleation event was disallowed. Thus, the effective nucleation rate reduced as the α volume fraction increased.

At a nucleation rate of 5 s⁻¹, the temporal evolution of α led to the formation of a basket weave structure for both 950 K and 1000 K (677 °C and 727 °C). The

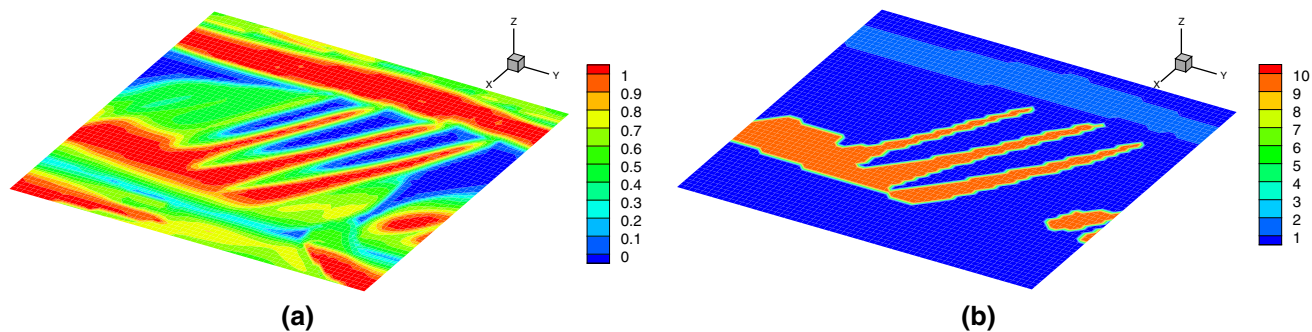


Fig. 7—Long-term evolution of the microstructure shown in Fig. 6. (a) contour plot of the sum of order parameters and (b) contour of variant numbers. Variant 10 is seen to nucleate in an autocatalytic fashion.

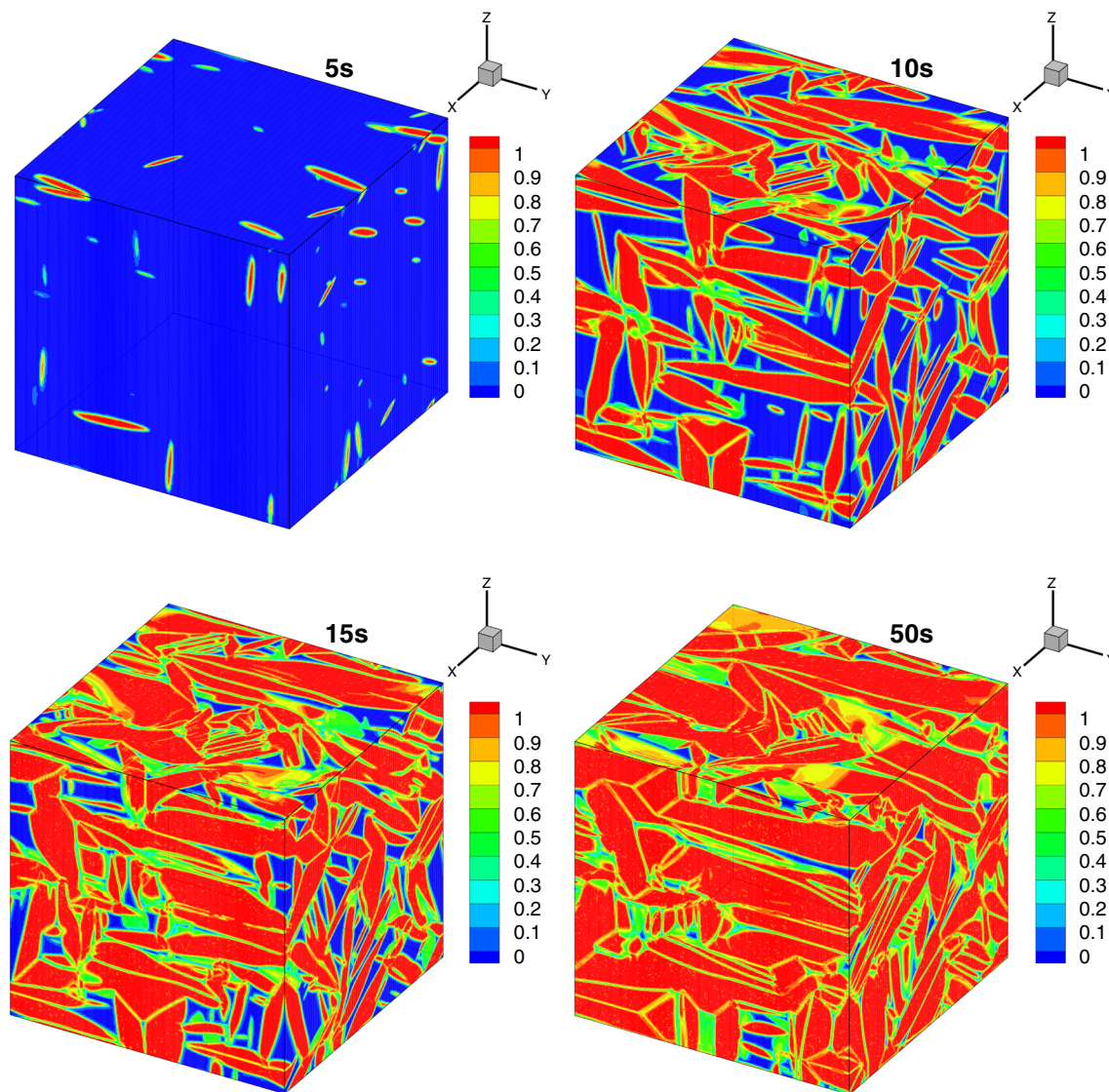


Fig. 8—Temporal evolution of α at 950 K (677 °C) with a nucleation attempt frequency of 5.0 s^{-1} showing the formation of multiple variants that results in a basket weave structure. Contours based on sum of order parameters.

temporal evolution of the basket weave morphology is shown in Figures 8 and 9 as contours of the sum of the order parameters. The simulations showed that for

both levels of thermodynamic undercooling, the high nucleation rate ensured that many composite nuclei were introduced into the β phase. The evolving strain

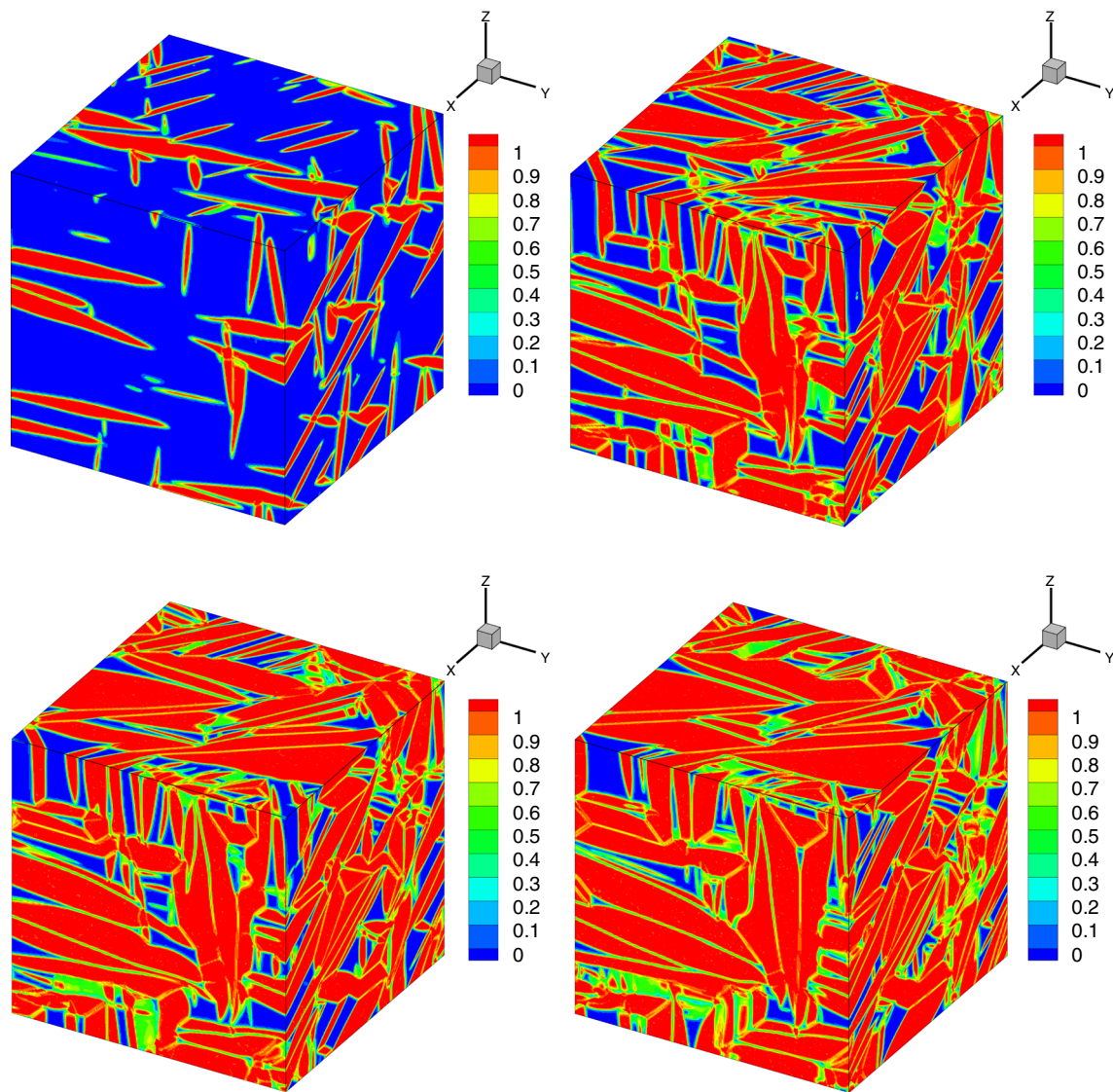


Fig. 9—Temporal evolution of α at 1000 K (727 °C) with a nucleation attempt frequency of 5.0 s^{-1} showing the formation of multiple variants that results in a basket weave structure. Contour based on the sum of the order parameters at each site.

field from many nearby composite nuclei influenced the variant that evolved from any single composite nucleus. Since it was shown earlier that the variant selection from the composite nucleus is based on strain energy minimization, the evolution criterion for the basket weave structure with multiple variants appears to be related to the strain accommodation mechanism similar to the one suggested by Sargent *et al.*,^[11] which minimizes the overall strain energy in the system. Representing the microstructure on the basis of the variant type in Figure 10 shows that almost all the variants are present in the microstructure. There is very little difference in morphologically between the final microstructures produced at 950 K and 1000 K (677 °C and 727 °C), except that the transformation at 1000 K (727 °C) is completed at an earlier time than at 950 K (677 °C) due to faster diffusion kinetics at 1000 K (727 °C).

When the nucleation attempt frequency is low (0.4 s^{-1}), the time between successive nucleation events is high. Therefore, there is sufficient time for a pre-nucleated variant to grow to a large size before subsequent nucleation occurs in its immediate vicinity. The preferential growth of a single variant from a composite nucleus, in this case, is governed by the strain fields associated with one or two nearby variants only. The simulations show that under these conditions the autocatalytic nucleation and growth similar to the one shown in Figure 5 occurs. The temporal evolution of the structure at 950 K (677 °C) is shown in Figure 11. For isothermal transformation at 950 K (677 °C), variant 11 is seen to grow in a lamellar fashion in the space between the previously grown variants as shown in Figure 12. The variant color map shows that the nearby variant in this case is 5. For isothermal transformation at 1000 K (727 °C), variant

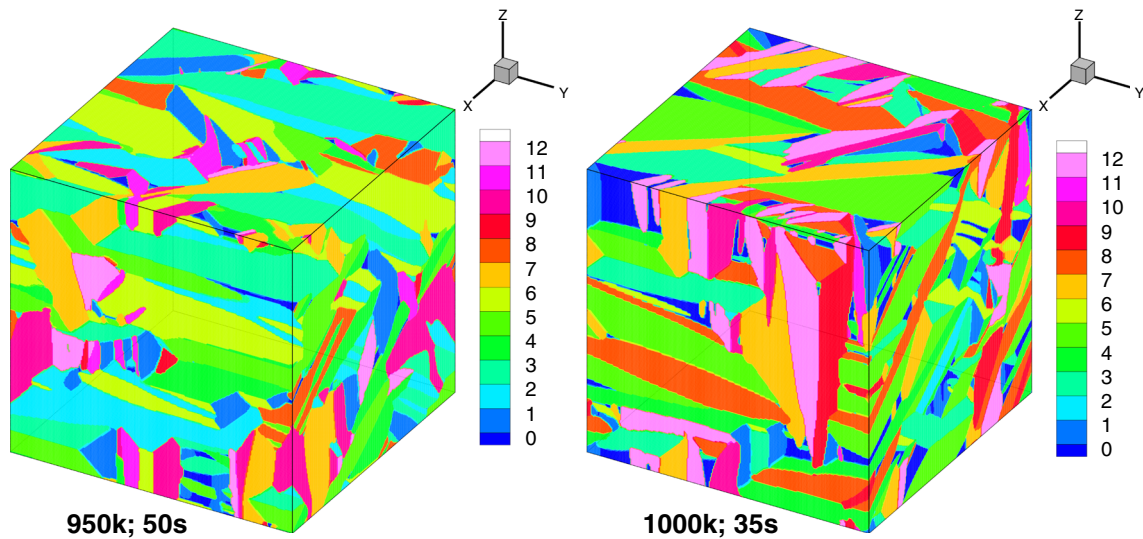


Fig. 10—Comparison of the basket weave structures obtained at 950 K and 1000 K (677 °C and 727 °C) at a nucleation attempt frequency of 5.0 s^{-1} using contours of variant numbers. Almost all variants are present in the microstructure.

1 forms as a colony when variant 12 surrounds it. It is clear that the variant that forms in the colony depends on the type of the surrounding variants and therefore a specific combination of elastic strains.

D. Relevance to Basket Weave to Colony Structure Transition During LAM of Ti-6Al-4V

LAM of Ti-6Al-4V involves melting powder in successive layers to form a part.^[6,7] As successive layers are melted, the previously solidified layers experience multiple thermal cycles as the laser source processes the top layer. The peak temperature at any location in the pre-solidified material decreases from the liquidus temperature to the $\beta \rightarrow \alpha$ transformation temperature as the subsequent layers build up. Although these temperatures are known to be a function of the heating and cooling rates, it is clear from the experiments of Kelley *et al.*^[6,7] that the so-called layer bands that contain the colony α morphology are formed only when the re-heat temperature exceeds the on-heating solvus temperature and the on-cooling transformation occurs in the diffusive regime. Outside the layer bands, a graded basket weave structure is seen with varying thickness of the α phase. The length scale of the α colony within the layer bands as well as the thickness of the layer bands is only tens of micrometers, while the prior β grains are of the order of millimeters. Therefore, the colony morphology should have resulted from an intragranular nucleation of α lamellae. No significant compositional inhomogeneity was found across the layer band and therefore should not play a role in the formation of the layer band.

Dislocations are known to form in metallic alloys due to rapid solidification^[33] and rapid thermal cycling.^[34,35] In the case of rapid solidification, it was shown that a high density of dislocations was grown into the solid during freezing of several metallic systems including nickel, copper, Ag-Cu alloys, and a DD3 single crystal

superalloy.^[33] A similar effect was observed in the weld heat-affected zone (HAZ) of the Ni-base superalloy TSM-75,^[34,35] where it was found that the dislocation generation involved a broad region of the fusion line that covered the solid as well as the liquid sides. The dislocation density was shown to increase by at least one order of magnitude over a distance of several millimeters. It was also shown that the dislocation density in the HAZ at a given distance from the fusion line increased with the cooling rate. A similar dislocation generation mechanism probably occurs during LAM. Accordingly, the dislocation content in the high-temperature β phase would be the highest near the fusion line and would decrease at distances farther down in the pre-solidified regions. Therefore in regions closer to the fusion line, the β phase could transform into a basket weave structure similar to the high nucleation rate case shown in Figures 8 through 10. Presumably, when the dislocation content falls below a threshold level, the critical nucleation rate required to sustain such a long-range strain relaxation mechanism cannot be sustained, and β phase would transform to a colony structure as shown in Figures 11 and 12. As the cooling rate reduces further, very little dislocation generation occurs. However, the peak temperatures are probably either in the $\alpha + \beta$ region or the dissolution of the α phase is not complete such that residual nuclei exist in the material which would again lead to a high effective nucleation rate. The assumption of two independent heterogeneous nucleation rates at each temperature in the current simulations is to represent two sets of process parameters with different levels of heat input. For the assumed nucleation rates and transformation temperatures, the transition from basket weave to columnar morphology seems to depend more on the nucleation rate than the transformation temperature.

While the dislocation density generated due to rapid cooling decreases monotonically from the fusion line, and therefore the heterogeneous nucleation rate on the

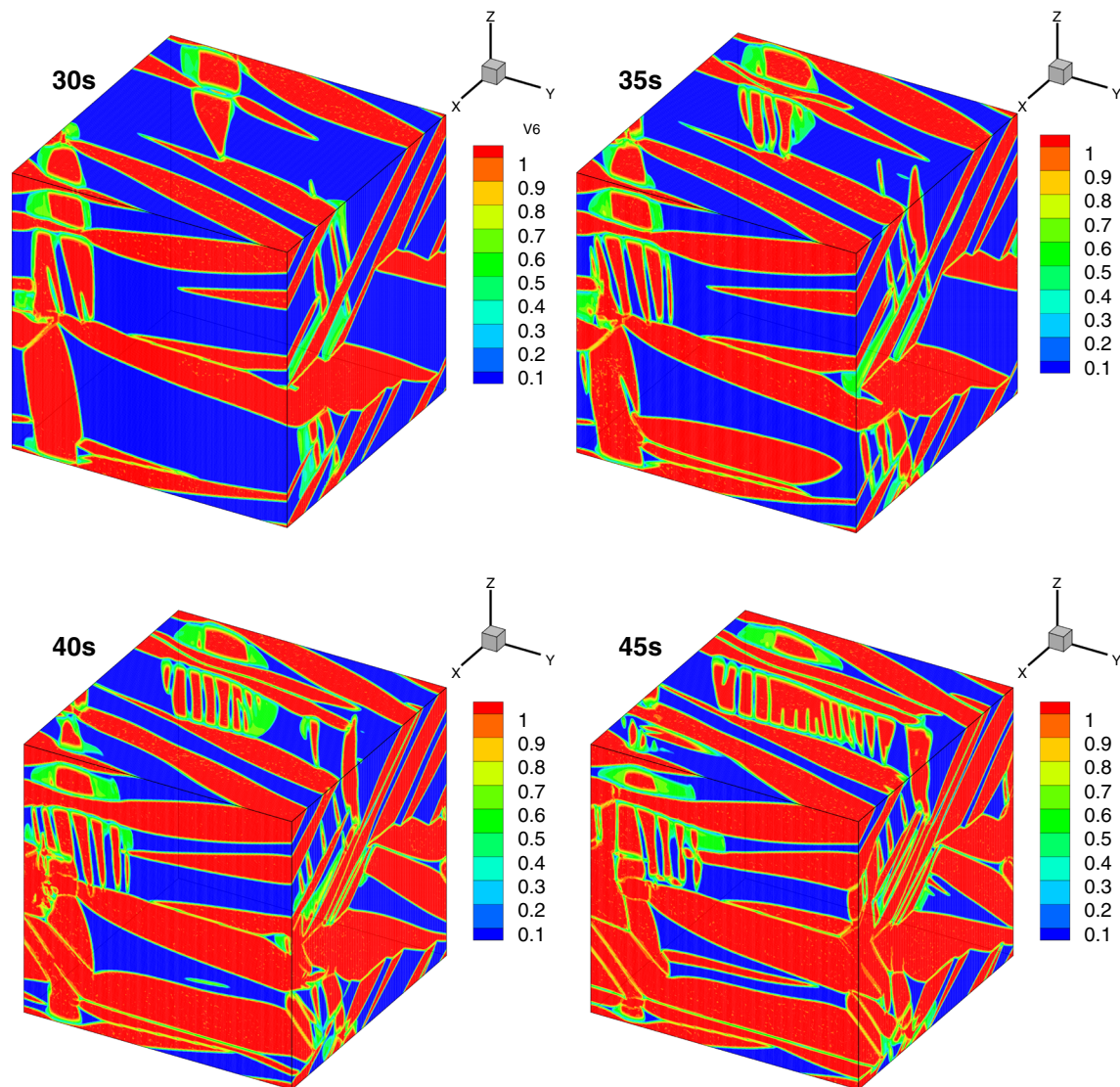


Fig. 11—Temporal evolution of α at 950 K (677 °C) at a nucleation attempt frequency of 0.4 s^{-1} showing autocatalytic nucleation of lamellae of the same variant. Colored according to the sum of the order parameters of variants at each site.

dislocations would also show a similar trend, homogeneous nucleation rate goes through a peak as a function of increasing undercooling (decreasing distance from the fusion line). Therefore, the assumption of homogeneous nucleation may not lead to a unique location of the layer band in the HAZ based on the nucleation rate-dependent mechanism described above. Since the homogeneous nucleation rate is maximum at a given undercooling, it would be lower at a higher or lower level of undercooling. Therefore, a zone with basket weave morphology would be sandwiched between two zones with a colony microstructure. However, this does not occur and the layer band is always confined to regions where the peak temperature is just above the $\beta \rightarrow \alpha$ transformation temperature. Therefore, variation in the heterogeneous nucleation rate due to a monotonic variation in the dislocation density as a function of peak

temperature in the HAZ is a more likely explanation for the layer bands.

However, in reality the thermal history of the material during LAM is much more complicated than the isothermal conditions for which the simulations are carried out. Each volume element is subjected to multiple thermal cycles where each subsequent thermal cycle has a lower peak temperature, and lower heating and cooling rates. The kinetics of dissolution of α and homogenization β depend on the heating and cooling rates and the total residence time above the β transition temperature. The on-heating and on-cooling transformation temperatures are therefore functions of solute diffusion kinetics. The heterogeneous nucleation rate will also become a function of the time-temperature history. Incorporating such complexities in phase field simulations will be the subject of future research.

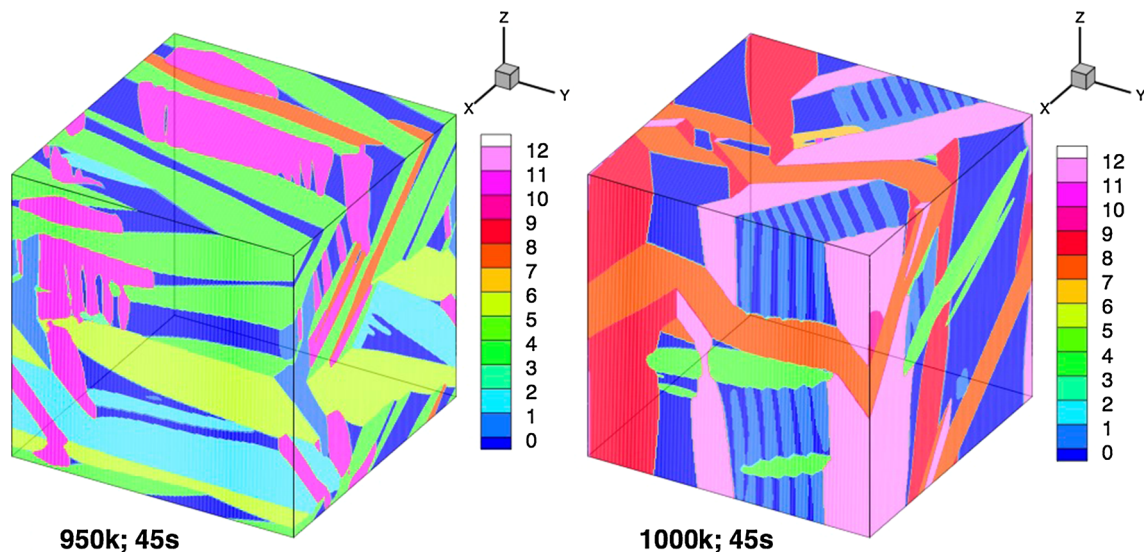


Fig. 12—Comparison of the variant morphologies obtained at a nucleation attempt frequency of 0.4 s^{-1} using contours of variant colors. At 950 K (677 °C), variant 11 exhibits autocatalytic nucleation, while at 1000 K (727 °C) variant 1 forms by autocatalytic nucleation.

V. SUMMARY AND CONCLUSIONS

Phase field simulations of $\beta \rightarrow \alpha$ transformation in Ti-6Al-4V in the diffusional transformation regime were carried out under the assumption of negligible V partitioning. The simulations considered the effect of the elastic strain fields due to transformation strains and their effect on variant selection during nucleation and growth of α . A composite nucleation model was used to represent heterogeneous nucleation of multiple variants due to pre-existing strain fields of dislocations. The subsequent variant selection due to strain fields of growing variants was investigated. The following conclusions were reached:

- (1) Strain fields due to pre-existing variants had a significant influence on variant selection from the composite nucleus whether the variant existed in a non-equilibrium orientation such as on a grain boundary or equilibrium orientations such as inside a grain based on a BO relationship.
- (2) Under certain combinations of pre-existing variants, an autocatalytic nucleation was observed that gave rise to colony α morphology.
- (3) The morphology evolution during nucleation and growth of multiple variants of α in a β grain was a function of the nucleation rate. At high nucleation rates, basket weave morphology was obtained, while at an order of magnitude lower nucleation rate autocatalytic nucleation and growth mechanism was observed that gave rise to the formation of lamellar α .
- (4) Heterogeneous nucleation model on pre-existing dislocations can offer a qualitative explanation for the formation of layer bands during LAM of Ti-6Al-4V.

ACKNOWLEDGMENTS

This research was sponsored by the Laboratory Directed Research and Development program at Oak Ridge National Laboratory, managed by UT-Battelle, LLC, under contract DE-AC05-00OR22725 for the U.S. Department of Energy. This research used resources of the Center for Computational Sciences at Oak Ridge National Laboratory, which is supported by the Office of Science of the U.S. Department of Energy under contract DE-AC05-00OR22725.

REFERENCES

1. N. Stanford and P.S. Bate: *Acta Mater.*, 2004, vol. 52, pp. 5215–24.
2. S.M. Kelly *et al.*, *Proceedings of the 7th International Conference on Trends in Welding Research*, May 16–20, 2005, Pine Mountain, GA, pp. 65–70.
3. R.D. Townsend and J.S. Kirkaldy: *Trans. ASM*, 1969, vol. 61, pp. 605–19.
4. H.I. Aaronson *et al.*: *Mater. Sci. Eng.*, 1995, vol. B32, pp. 107–23.
5. R. Shi and Y. Wang: *Acta Mater.*, 2013, vol. 61, pp. 6006–24.
6. S.M. Kelly and S.L. Kampe: *Metall. Mater. Trans. A*, 2004, vol. 35A, pp. 1861–67.
7. S.M. Kelly and S.L. Kampe: *Metall. Mater. Trans. A*, 2004, vol. 35A, pp. 1869–79.
8. D. Qiu, R. Shi, D. Zhang, W. Lu, and Y. Wang: *Acta Metall.*, 2015, vol. 88, pp. 218–31.
9. Y. Liao *et al.*: *J. Appl. Phys.*, 2010, vol. 108, p. 063518.
10. J.W. Christian: *The Theory of Transformations in Metals and Alloys—Part 1*, Pergamon, Oxford, 2002.
11. G.A. Sargent *et al.*: *Metall. Mater. Trans. A*, 2012, vol. 43A, pp. 3570–85.
12. R.V. Ramanujan and P.J. Maziasz: *Metall. Mater. Trans. A*, 1996, vol. 27A, pp. 1661–73.
13. S.G. Kim, W.T. Kim, and T. Suzuki: *Phys. Rev. E*, 1999, vol. 60, pp. 7186–97.
14. I. Steinbach and M. Apel: *Physica D*, 2006, vol. 217, pp. 153–60.
15. H. Kobayashi *et al.*: *Scripta Mater.*, 2003, vol. 48, pp. 689–94.
16. L.Q. Chen: *Annu. Rev. Mater. Res.*, 2002, vol. 32, pp. 113–40.

17. N. Moelans, B. Blanpain, and P. Wollants: *Calphad*, 2008, vol. 32, pp. 268–94.
18. A.G. Khachaturyan: *Theory of structural transformations in solids*, Wiley, New York, 1983, pp. 226–40.
19. K. Ammar, B. Appolaire, G. Cailletaud, and S. Forest: *Eur. J. Comput. Mech.*, 2009, vol. 18, pp. 485–523.
20. S.Y. Hu and L.Q. Chen: *Acta Mater.*, 2001, vol. 49, pp. 1879–90.
21. J.L.W. Warwick *et al.*: *Acta Mater.*, 2012, vol. 60, pp. 4117–27.
22. I. Katzarov, S. Malinov, and W. Sha: *Metall. Mater. Trans. A*, 2002, vol. 33A, pp. 1027–40.
23. C.G. Rhodes and N.E. Paton: *Metall. Mater. Trans. A*, 1979, vol. 10A, pp. 209–16.
24. Y. Ohmori, K. Nakai, H. Ohtsubo, and M. Tsunofuri: *Mater. Trans. JIM*, 1994, vol. 35, pp. 238–46.
25. T. Ahmed and H.J. Rack: *Mater. Sci. Eng.*, 1998, vol. A243, pp. 206–11.
26. Y. Ji *et al.*: *J. Phase Equilib. Diffus.*, 2016, vol. 37, pp. 53–64.
27. S.L. Semiatin *et al.*: *Metall. Mater. Trans. A*, 2004, vol. 35A, pp. 3015–18.
28. D. Good: *J. Inst. Met.*, 1959–1960, vol. 88, pp. 444–48.
29. L.-Q. Chen and J. Shen: *Comput. Phys. Commun.*, 1998, vol. 108, pp. 147–58.
30. D. Pekurovsky: *SIAM J. Sci. Comput.*, 2012, vol. 34, pp. C192–C209.
31. T.W. Heo and L-Q.Chen: *JOM*, 2014, vol. 66, pp. 1520–28.
32. R. Shi, N. Ma, and Y. Wang: *Acta Mater.*, 2012, vol. 60, pp. 4172–84.
33. F. Diu, D.W. Zhao, and G.C. Yang: *Metall. Mater. Trans. B*, 2001, vol. 32B, pp. 449–57.
34. O.M. Barabash *et al.*: *J. Appl. Phys.*, 2003, vol. 94, pp. 738–42.
35. O.M. Barabash *et al.*: *J. Appl. Phys.*, 2004, vol. 96, pp. 3673–79.